analytical chemistry

pubs.acs.org/ac Article

Nanoscale Carbonate Ion-Selective Amperometric/Voltammetric Probes Based on Ion−Ionophore Recognition at the Organic/Water Interface: Hidden Pieces of the Puzzle in the Nanoscale Phase

Subhashini Elangovan, Surendra Raj Puri, Hiranya Madawala, Justin Pantano, Brett Pellock, Matthew K. Kiesewetter, and Jiyeon Kim*

Cite This: *Anal. Chem.* 2023, 95, 4271−4281 Read Online

ACCESS | Metrics & More | Article Recommendations | Supporting Information

ABSTRACT: Here, we report on the successful demonstration and application of carbonate (CO_3^{2-}) ion-selective amperometric/voltammetric nanoprobes based on facilitated ion transfer (IT) at the nanoscale interface between two immiscible electrolyte solutions. This electrochemical study reveals critical factors to govern CO_3^{2-}-selective nanoprobes using broadly available Simon-type ionophores forming a covalent bond with CO_3^{2-}, i.e., slow dissolution of lipophilic ionophores in the organic phase, activation of hydrated ionophores, peculiar solubility of a hydrated ion−ionophore complex near the interface, and cleanness at the nanoscale interface. These factors are experimentally confirmed by nanopipet voltammetry, where a facilitated CO_3^{2-} IT is studied with a nanopipet filled with an organic phase containing the trifluoroacetophenone derivative CO_3^{2-}ionophore (CO_3^{2-}ionophore VII) by voltammetrically and amperometrically sensing CO_3^{2-} in water. Theoretical assessments of reproducible voltammetric data confirm that the dynamics of CO_3^{2-} ionophore VII-facilitated ITs (FITs) follows the one-step electrochemical (E) mechanism controlled by both water-finger formation/dissociation and ion−ionophore complexation/dissociation during interfacial ITs. The yielded rate constant, k^0 = 0.048 cm/s, is very similar to the reported values of other FIT reactions using ionophores forming non-covalent bonds with ions, implying that a weak binding between CO_3^{2-} ion−ionophore enables us to observe FITs by fast nanopipet voltammetry regardless of the nature of bondings between the ion and ionophore. The analytical utility of CO_3^{2-}-selective amperometric nanoprobes is further demonstrated by measuring the CO_3^{2-} concentration produced by metal-reducing bacteria *Shewanella oneidensis* MR-1 as a result of organic fuel oxidation in bacterial growth media in the presence of various interferents such as $H_2PO_4^-$, Cl^-, and SO_4^{2-}.

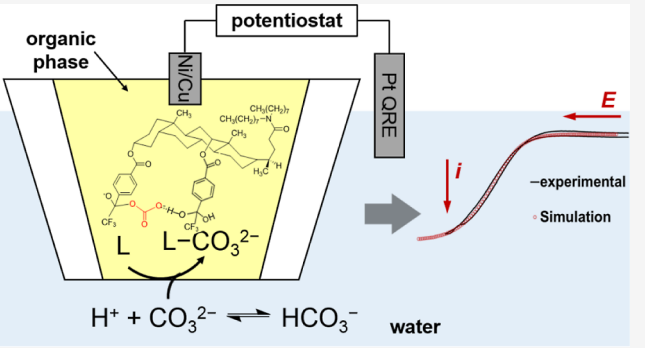

1. INTRODUCTION

Selective ion transfer (IT) at a liquid/liquid interface has been extensively applied for electrochemical sensing of redox-inactive ions or ionized biomolecules critical for clinical,[1] physiological,[2] industrial,[3] and environmental analysis.[4] While potentiometric ion-selective electrodes (ISEs) have been the most common approach with measuring a change in phase boundary potential upon equilibrated analyte partitioning between two liquid phases,[5−8] amperometric/voltammetric ISEs have steadily emerged owing to the high sensitivity.[9,10] In fact, current responses of amperometric ISEs directly depend on the analyte concentration, whereas potential responses of potentiometric ISEs are varied with the logarithm of the concentration.[5,6,11] This high sensitivity of the amperometric/voltammetric approach is more suitable to study heterogeneously distributed analyte ions in the system by catalytic production, consumption, or other chemical reactions than potentiometric ISEs.[12−14]

A glass pipet-supported interface between two immiscible electrolyte solutions (ITIES) has played a critical role in studying IT dynamics at liquid/liquid interfaces for both simple and facilitated ITs (FITs). For FITs, ion-selective ionophores existing inside or outside a pipet facilitate the thermodynamically unfavorable transfer of hydrophilic ions from an aqueous solution to an organic phase.[15,16] As pipets are readily pulled to micro−nanometer sizes, ion-selective amperometric/voltammetric probes could be easily miniaturized up to the nanometer scale. Especially, a small current across a pipet-supported interface enables not only a reliable

Received: June 19, 2022
Accepted: February 8, 2023
Published: February 21, 2023

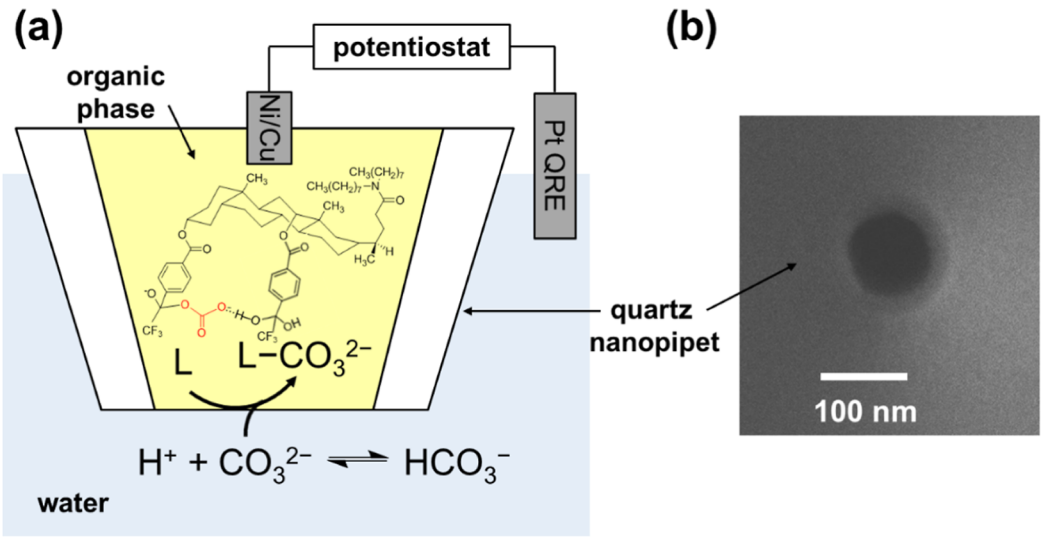

Figure 1. (a) Schematic view of a facilitated CO_3^{2-} ion transfer at a water/1,2-DCE interface measured by nanopipet voltammetry/amperometry. (b) SEM image of an orifice of a silanized nanopipet with a ca. 3 nm thick Au layer coated by an Au sputter coater. The SEM image was obtained using an accelerating voltage of 5 kV to minimize charging up.

study of IT dynamics due to a negligibly small ohmic potential drop[17] but also a spatially resolved study of IT with a combination of scanning electrochemical microscopy (SECM).[18] Accordingly, the anticipated advantages from a nanoscopic interface using a nanopipet are obvious, which enables the determination of large IT rate constants owing to fast mass transfer[19−22] and mapping heterogeneous distribution of analyte ions with SECM at a high spatial resolution of nanoscale.[23,24] So far, most studies in FITs have been focused on the microscale interface using micro-sized pipets, whereas very few innovative works using nanopipets were reported.[19−25] Especially, the nanoscopic study of an FIT using nanopipets has been rare with broadly available ionophores a.k.a., Simon's ionophores developed by Wilhelm Simon,[26] having a large molecular weight (∼1000 or larger) and high lipophilicity. We suspect that reproducibility and stability could be main challenges in this nanoscale amperometric/voltammetric study. Since the active area of the nanopipet interface is small, it is susceptible to adventitious contaminants or precipitate, thus being easily blocked. Accordingly, the stability and reproducibility of current responses could rely on the control of these two factors, contaminants and precipitate at the nanoscale interface.

The visual characterization of an intact nanopipet interface related to contaminant and precipitate issue is technically limited due to the small size and the liquid phase interface, which makes empirical control of these factors complicated and even puzzling. We investigate the CO_3^{2-}-selective IT system as a model and study FITs using nanopipet-supported ITIES with the voltammetry technique to demonstrate the origins of hampering factors in this amperometric nano-ISE. In this system, interfacial CO_3^{2-} IT across the water/organic interface supported by a nanopipet is facilitated by the CO_3^{2-}-selective ionophore dissolved in the organic phase inside a pipet (Figure 1). A molecular tweezer-type ionophore, *N*,*N*-dioctyl-3α,12α-bis(4-trifluoroacetylbenzoyloxy)-5β-cholan-24-amide (a.k.a., CO_3^{2-} ionophore VII), has two trifluoroacetophenone groups interacting selectively with CO_3^{2-} to form a 1:1 complex with a mixture of covalent and hydrogen bonding (see Figures 1a and S1).[27,28] In the presence of excess ionophore in the inner solution, conventional steady-state voltammograms can be observed for this FIT, where mass transfer is controlled by hemispherical diffusion of CO_3^{2-} ions in the outer aqueous solution.[29] Herein, our nanoelectrochemical study focuses on four critical factors such as slow dissolution of the bulky lipophilic ionophore in the organic phase, activation of hydrated ionophores, peculiar solubility of the lipophilic ionophore and ion−ionophore complex in the organic phase near the interface, and cleanness at the nanoscale interface. All factors are directly related with the blockage of the nanoscale liquid/liquid interface, thus determining the stability and reproducibility of current responses during FITs, i.e., the performance of amperometric nano-ISEs. Accordingly, resulting steady-state voltammograms should be evaluated for continuity and stability of current responses, reproducibility during repetitive measurements, and validity of the FIT kinetics and mechanism.

CO_3^{2-} sensing by amperometric nano-ISEs can be broadly applied to study not only total CO_2 in physiological fluids, oceanic carbonate systems, and industrial samples but also renewable energy systems such as organic fuel oxidation by dissimilatory metal-reducing bacteria (MRB) used for microbial fuel cells (MFCs),[30] and electrocatalytic reduction of CO_2 to organic fuel carried by a carbonate solution.[31] Pioneering works on CO_3^{2-}-selective potentiometric sensing using CO_3^{2-} ionophore VII have been reported by the Bakker group and Nam group to determine the CO_2 (or CO_3^{2-}) concentration in aqueous/gaseous samples and oceanic carbon dioxide in seawater, which are suitable to investigate bulk samples from physiological fluids, fresh water systems, or oceanic carbonate systems.[27,28,32−38] However, the study of organic fuel oxidation by MRB at an individual cell or electrochemical reduction of CO_2 at an individual heterogeneous nanocatalyst requires both high sensitivity and miniaturization to the nanoscale of CO_3^{2-} ISEs. For example, the quantitative measurement of how fast organic fuel is oxidized at a single MRB is a crucial part to fundamentally understand the rate-determining step in the electron transport pathway of MRB, which determines the overall efficiency of MFCs.[39,40] This can be accomplished by real-time measuring CO_3^{2-} production over a single bacterium

https://doi.org/10.1021/acs.analchem.2c02626
Anal. Chem. 2023, 95, 4271−4281

using amperometric nano-ISEs. Also, the catalytic activity of individual heterogeneous nanocatalysts for CO_2 reduction can be evaluated by measuring how fast and efficiently CO_3^{2-} is consumed and converted over each discrete catalyst. Particularly, high spatial resolution as well as intrinsically high sensitivity of amperometric nano-ISEs can be combined with SECM to reveal active sites in heterogeneous target samples and establish the relationship between the structure and reactivity of a single object. Despite these analytical potentials, none of studies about amperometric nano-CO_3^{2-} ISEs have been reported so far.

Here, we report on the successful demonstration and application of amperometric CO_3^{2-}-ISEs based on FIT at the nanopipet-supported ITIES using the "Simon" type ionophore (CO_3^{2-} ionophore VII) forming a covalent bond with CO_3^{2-}. Nanopipet voltammetry is performed to clarify the hampering factors in realizing nanoscale CO_3^{2-}-ISEs. Reproducible voltammetric data obtained are theoretically assessed to verify the dynamics and mechanism of the CO_3^{2-}-ionophore-FIT. The quantitative analysis yields a normal α value of 0.45 and a rate constant, k^0 0.048 cm/s, in a one-step electrochemical (E) mechanism controlled by both water-finger formation/dissociation and ion−ionophore complexation/dissociation during interfacial IT.[41−43] This k^0 based on the E mechanism is more reasonable than unrealistically fast interfacial IT rate constant, k^0 = 35 cm/s, and an association rate constant, k_a = 3.3×10^{20} M^{-1} s^{-1}, exceeding diffusion limits in the two step-electrochemical-chemical (EC) mechanism based on the simple interfacial transfer of CO_3^{2-} followed by complexation in the organic phase, thereby excluding the EC mechanism for our quasi-reversible FIT at nano-ITIES (Table S7 in the Supporting Information). Notably, the obtained k^0 in the E mechanism is very similar to reported values of other FITs at microscale ITIES using non-covalent bond-forming ionophores,[16] implying that a weak binding of CO_3^{2-} ion−ionophore enables us to observe FITs in fast nanopipet-voltammetric measurements regardless of the nature of bonding. We further employed a fundamentally proved nanoscale CO_3^{2-}-ISE to sense and quantify CO_3^{2-} produced by MRB, e.g., *Shewanella oneidensis* MR-1 as a result of organic fuel oxidation, thus demonstrating its analytical applicability as well.

2. EXPERIMENTAL SECTION

2.1. Chemicals. Ammonium carbonate [$(NH_4)_2CO_3$], tetrabutylammonium chloride (TBA^+Cl^-), ammonium phosphate monobasic ($(NH_4)H_2PO_4$), ammonium phosphate dibasic [$(NH_4)_2HPO_4$], *N*,*N*-dimethyltrimethylsilylamine, 1,2-dichloroethane (DCE), 1,2-dichloromethane, isopropyl alcohol, tetradodecylammonium bromide (TDDABr), acetic acid, and nitric acid were purchased from Sigma-Aldrich and used as obtained. Potassium tetrakis(pentafluorophenyl)-borate (KTFPB) was purchased from Boulder Scientific. Ionic liquid-supporting electrolytes ($TDDA^+{}^{\bullet}TFPB^-$ or TDDATFPB) are prepared by metathesis of TDDABr and KTFPB.[44] More details about the metathesis are in the Supporting Information (SI). *N*,*N*-Dioctyl-3α,12α-bis(4-trifluoroacetylbenzoyloxy)-5β-cholan-24-amide (CO_3^{2-} ionophore VII) was used as purchased from Sigma-Aldrich. Modified M-1 medium for *Shewanella* federation was prepared and provided by the Pellock group, and the recipe of modified M-1 medium is presented in detail in the Supporting Information.

2.2. Fabrication of Nanopipet Electrodes. Nanopipets were pulled from a quartz capillary (outer diameter = 1 mm, inner dimeter = 0.7 mm, length = 10 cm, FG-GQ100-70-10, Sutter Instrument Co., Novato, CA) using a CO_2 −laser puller (P-2000, Sutter Instrument Co., Novato, CA). As-pulled nanopipets were further silanized for electrochemical measurements. A DCE solution containing 30 mM CO_3^{2-} ionophore VII and 0.1 M TDDATFPB is prepared by vortexing for 15 min up to 3 h for thorough dissolution. (There was no difference between the 15 min and 3 h vortexing, data not shown.) The silanized pipet is filled with either a freshly prepared DCE solution or a premade one aged for ∼12 h. An electrochemically etched Ni/Cu wire as an inner reference electrode is inserted from the back opening of a nanopipet and immobilized at the position of ca 200 μm from the tapered tip end (details about the silanization setup and procedure and fabrication of inner reference electrodes are in the Supporting Information).

2.3. Nanopipet Characterization by Scanning Electron Microscopy. As-pulled quartz nanopipets were characterized by scanning electron microscopy (SEM) (SIGMA VP field emission scanning electron microscope, Zeiss). Before SEM measurements, the pipet surface was sputter-coated with ca 3 nm thick Au layer to suppress the charging up (Cressington Au sputter coater 108 auto equipped with Cressington thickness monitor mtm10, Ted Pella INC, Redding, CA, USA). The sputtered Au thickness can be monitored in situ with the aid of an equipped thickness monitor (Cressington thickness monitor mtm10), thereby optimizing the sputtering condition with 20 mA current, 10 s sputtering time, and resulting thickness of 3.4−3.7 nm. The orifice of nanopipets was observed using e-beam with a 5 kV accelerate voltage (Figure 1b).

2.4. NMR Experiments. All NMR experiments were performed using a Bruker ASCEND 400 MHz spectrometer at 298 K. A capillary of 0.010 M hexafluorobenzene (HFB) in DMSO-d_6 was prepared as an internal standard. ^1H spectra were referenced to the solvent residual signal and collected using standard acquisition parameters. ^{19}F spectra were referenced to HFB and collected using an acquisition delay of 30 s. Samples prepared for analysis included 30 mM ionophore VII in DCE, a 0.100 M ionic liquid in DCE, and a combination of 30 mM ionophore and 0.100 M ionic liquid in DCE.

2.5. Electrochemical Measurements. Electrochemical workstations (CHI 8022D and CHI 760E, CH Instruments, Austin, TX) were used for voltammetric and amperometric measurements. Nanopipet voltammetry employed two-electrode cells using a Pt-wire (0.5 mm, hard, 99.95%, Alfa Aesar) as a quasi-reference electrode (QRE) as represented by the Pt QRE| CO_3^{2-} ion and TBA^+ ion with supporting electrolytes in 40 mM phosphate buffer or M-1 medium (w)|30 mM CO_3^{2-} ionophore VII and 0.1 M TDDATFPB (DCE)|Ni/Cu (more details are in the Supporting Information).

2.6. Standard Addition Method for Quantification of the CO_3^{2-} Level Produced by *S. oneidensis*. To quantify the CO_3^{2-} concentration produced by *S. oneidensis* as a result of oxidation of various carbon sources, we performed the standard addition method as well as nanopipet voltammetry. 30 mM of CO_3^{2-} stock solution prepared with fresh modified M-1 medium was added sequentially as spikes into the M-1 medium used for bacterial growth, which contained 30 mM lactate or 30 mM acetate with or without fumarate,

https://doi.org/10.1021/acs.analchem.2c02626
Anal. Chem. 2023, 95, 4271−4281

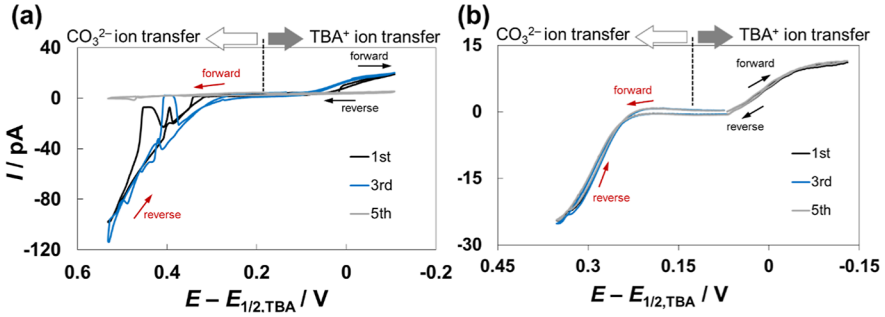

Figure 2. (a) Voltammograms with a CO_3^{2-}-selective nanopipet electrode filled with *freshly prepared* 30 mM ionophore solution under repetitive running of voltammetry (For CO_3^{2-} IT, potentials are scanned from 0.1 V to 0.55 V and back to 0.1 V. For TBA$^+$ IT, potentials are scanned from 0.1 to −0.15 V and back to 0.1 V). Within five runs, the nanopipets were completely blocked with showing a zero current response for both TBA$^+$ and CO_3^{2-} IT reactions (gray curve). (b) Voltammograms with a CO_3^{2-}-selective nanopipet electrode filled with a *premade* 30 mM ionophore solution under repetitive running of voltammetry. Repetitive runs showed reproducible current responses for both TBA$^+$ and CO_3^{2-} IT reactions. The scan rate for both measurements was 25 mV/s. All ionophore solutions were vortexed for 15 min.

respectively. The subsequent voltammetry was conducted to measure the ionic currents caused by CO_3^{2-} FIT. A calibration plot of limiting currents obtained from background-subtracted voltammograms vs added CO_3^{2-} concentrations was constructed, which resulted in a linear curve. Particularly, the *x*-intercept of this resulting plot directly corresponds to the original concentration of CO_3^{2-} intrinsically produced by *S. oneidensis*.[45] More details are in the Supporting Information.

2.7. Molecular Dynamics Simulations. The molecular structures of the CO_3^{2-} ion, CO_3^{2-} ionophore VII, water, and $CHCl_3$ were designed, and each conformation with minimum energy was also found using the MOE (MOE2020, Molecular Operation Environment) software under the program of the Merc-molecular force field (MMFF). More details are in the Supporting Information.

3. RESULTS AND DISCUSSION

3.1. Slow Dissolution of the Bulky Ionophore in the Organic Phase and Peculiar Solubility Origin at the Nanoscale Interface. A homogeneous DCE solution containing a 30 mM CO_3^{2-} ionophore was prepared with vortexing for 15 min prior to usage, which showed neither precipitation nor a separated layer. With this fresh DCE inner filling solution, a nanopipet electrode was fabricated by inserting an electrochemically etched Pt wire as an inner reference electrode. Subsequently, nanopipet voltammetry was performed in the aqueous bulk solution containing TBA$^+$ and CO_3^{2-}, where a simple TBA$^+$ IT was monitored in the negative potential scans to characterize a nanopipet, and a CO_3^{2-} FIT was studied in the positive potential scans. Within five runs, a nanopipet was totally blocked and thus, ionic current responses from both TBA$^+$ and CO_3^{2-} ITs disappeared (gray curves, Figure 2a). These sudden blockages of pipets were observed reproducibly during repetitive voltammetric measurements (100% failure with $n > 50$, data not shown). Notably, when the ionophore concentration was reduced to 5 mM, the blockage of nanopipets filled with the freshly prepared ionophore solution was mitigated with showing nearly reproducible TBA$^+$ ITs and yet hardly resolved CO_3^{2-} FITs (Figure S5). These results clearly imply that solubility of the ionophore in the DCE solution would be a critical factor in the observed FITs.

In fact, dissolution is not an instantaneous process. Under the diffusion-limiting process, the dissolution rate of a solid solute is dependent on its surface area and the diffusion coefficient as well as the concentration gradient between the solid surface (or saturated) and bulk solution as described by the Noyes−Whitney equation[46]

$$\frac{dC}{dt} = \frac{D \cdot s}{d}(C_s - C_b) \quad (1)$$

where dC/dt is the dissolution rate, t is the time, D is the diffusion coefficient of the solute in the solution, s is the surface area of the dissolving solute exposed in the solvent, d is the thickness of the diffusion layer, i.e., the thickness of the boundary layer of the solvent between the surface of the dissolving substance and the bulk, C_s is the concentration of the solute at the solid surface (or saturated), and C_b is the concentration of the solute in the bulk solution. Especially for a bulky solute like CO_3^{2-} ionophore VII dissolved in fairly viscous DCE solution, a small magnitude of D is anticipated by the Stokes−Einstein equation below[47]

$$D = \frac{kT}{6\pi\eta r} \quad (2)$$

where k is the Boltzmann constant, T is the absolute temperature, η is the viscosity of solution, and r is the radius of the solute molecule. Hence, small magnitudes of D and solute surface area, s, of a bulky ionophore would lead to a decrease in the overall dissolution rate (eq 1). This intuitive speculation, however, is not trivial since an amperometric nano-ISE with highly lipophilic Simon type ionophores has been often fouled unknowingly, and its utilization has been rare to happen.[48]

30 mM CO_3^{2-} ionophore VII in DCE is obviously excessive compared to the level of CO_3^{2-} studied, necessary for steady-state measurements. As CO_3^{2-} ionophore VII is highly lipophilic, an intrinsically high solubility in DCE solution is anticipated. In MD simulation, the solvation of the ionophore in the organic phase has a large negative value of free energy, thus being thermodynamically favorable (Tables S5 and S6).

However, our repetitive failures in realizing amperometric nano-ISEs with nanopipet voltammetry call attention to a need for a better understanding of the distinctive solubility of the lipophilic ionophore and its ion-complex in the organic phase. Subsequently, the solubility origin at the nanoscale in nonpolar environments was reconsidered. Earlier, Fileti and Chaban performed classical MD simulations and predicted the decrease in solvation of arbitrary nanostructures due to unfavorable entropic contributions instead of favorable enthalpic contributions, as their dimension becomes ca 2 nm or smaller.[49] A

https://doi.org/10.1021/acs.analchem.2c02626
Anal. Chem. 2023, 95, 4271−4281

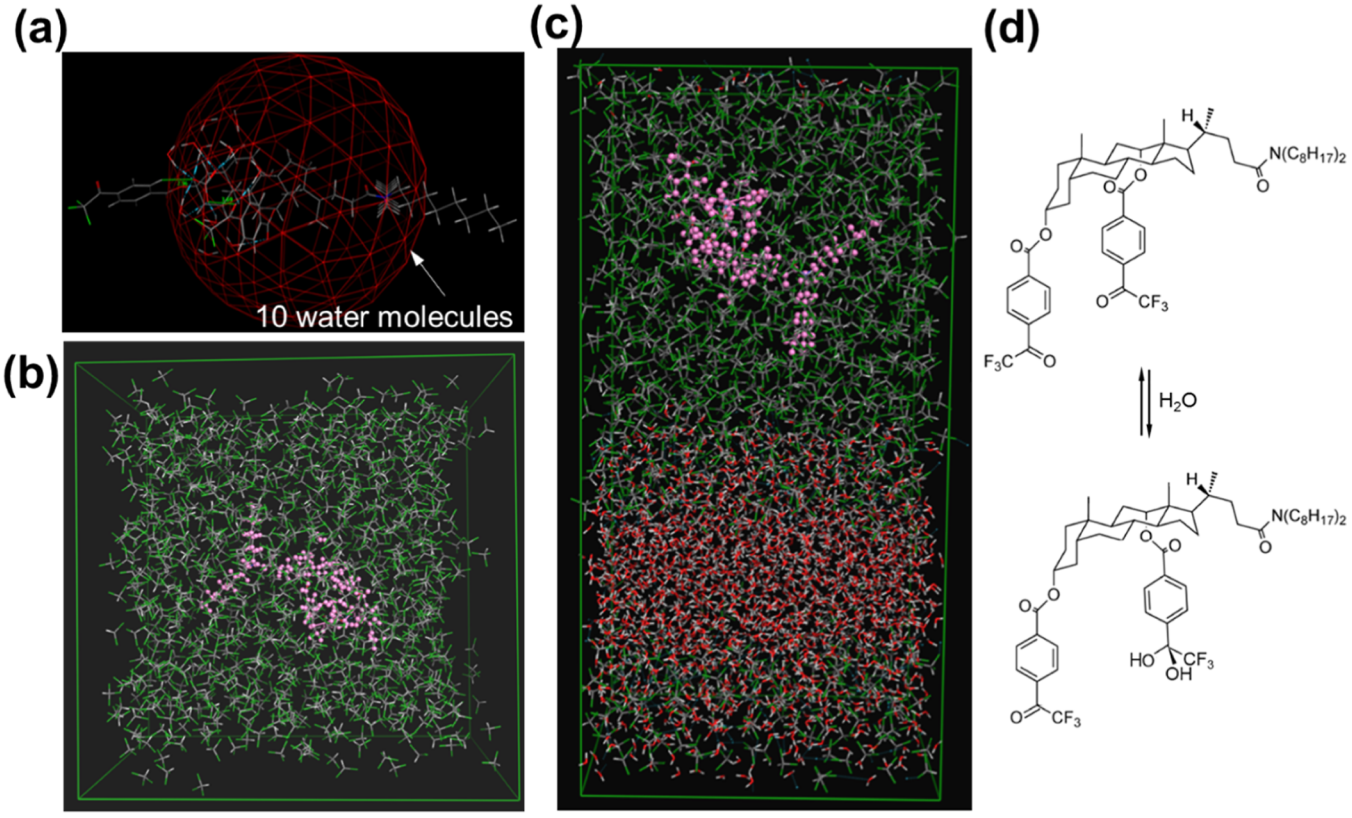

Figure 3. Snapshots of a (a) complex of CO_3^{2-} ionophore VII and a partially hydrated CO_3^{2-} ion surrounded by 10 water molecules. The red circle represents 10 water molecules surrounding the CO_3^{2-} ion. (b) Complex of CO_3^{2-} ionophore VII with CO_3^{2-} surrounded by 10 water molecules solvated in the $CHCl_3$ organic monophase. CO_3^{2-} ionophore VII is depicted with magenta balls, and the chloride atoms of $CHCl_3$ are shown in green. (c) A complex of CO_3^{2-} ionophore VII with CO_3^{2-} surrounded by 10 water molecules is solvated in the $CHCl_3$ organic phase near the water/$CHCl_3$ interface. CO_3^{2-} ionophore VII is depicted with magenta balls. The oxygen atoms of water are shown in red, and the chloride atoms are shown in green. (d) Hydration of trifluoroacetyl ketone of CO_3^{2-} ionophore VII.

sharp positive increase in the solvation free energy from ca 2 to 0.2 nm of the nanostructures is predicted due to lower conformational diversity of solvent−solute interactions in the solution, thereby decreasing the solvation entropy.[49] This theoretical speculation is consistent with our experimental observation of blocked current responses from nanopipets filled with DCE solution containing neutral lipophilic CO_3^{2-}-ionophore VII smaller than 2 nm. Hence, we suspected a decrease in the solubility of nanosized ionophores near the interface, which could transiently cause a local precipitation and the subsequent blockage of a nanopipet interface.

Moreover, the solubility of the ion−ionophore complex near the organic/water interface at the nanoscale should be differentiated from that in the bulk organic phase. An FIT occurs across the interface from water to the organic phase, where a hydrated ion forms an adduct with water molecules, so called a water-finger.[41,50,51] The water-finger formation/dissociation during interfacial ITs has been suggested by various groups based on theoretical and experimental approaches.[42,43,43,52−54] The breakage of the water-finger leaves a partially hydrated ion surrounded by an average of 10 water molecules in the organic phase,[41] which further undergoes a complexation with the ionophore.[43,52,53]

To elucidate the effect of partial hydration on the solubility of an ion−ionophore near the interface, we performed MD simulations using the MOE software under the program of MMFF. The solvation free energies of a complex between CO_3^{2-} ionophore VII and CO_3^{2-} in the organic monophase ($CHCl_3$) were calculated, where both free CO_3^{2-} and partially hydrated CO_3^{2-} with 10 water molecules were studied. Compared to a complex of CO_3^{2-} ionophore VII and free CO_3^{2-}, the free energy of a complex of CO_3^{2-} ionophore VII with partially hydrated CO_3^{2-} merely increases to positive, ca 1.6% (Figure 3b and Table S5 in Supporting Information). Within the diphase system, however, the free energy of CO_3^{2-} ionophore VII complexed with partially hydrated CO_3^{2-} dissolved in $CHCl_3$ showed ca 8.5% positive increase compared to that of free CO_3^{2-} ionophore VII dissolved in $CHCl_3$ (Figure 3c and Table S5 in the Supporting Information). Because of an exponential dependence of solubility on the free energy, i.e., $K \sim \exp(-\Delta G)$, even a moderate increase of the free energy leads to a significant decrease in solubility.[49] Resultantly, the decrease in the solubility of an ion−ionophore complex near the organic/water interface could hamper our voltammetric study of an FIT across the nanoscale interface.

Based on the speculation on the slow dissolution and the distinct solubility at the nanoscale interface, sufficient time for CO_3^{2-} ionophore VII solvation in DCE was given by preparing the DCE solution with up to 15 min of vortexing and storing on the laboratory bench for 9−12 h before usage. In nanopipet voltammetry, nanopipet electrodes filled with this premade ionophore solution successfully showed current responses for the CO_3^{2-} FIT in the positive potential scan and a simple TBA^+ IT occurred in the negative potential scan (Figure 2b). Conspicuously, each corresponding IT reaction was driven

https://doi.org/10.1021/acs.analchem.2c02626
Anal. Chem. 2023, 95, 4271−4281

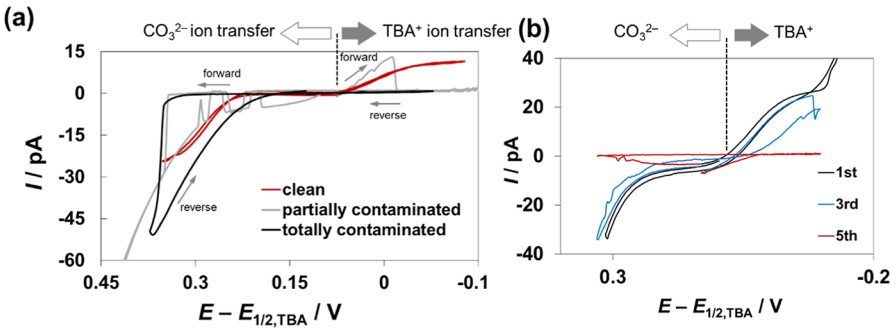

Figure 4. (a) CO_3^{2-}-selective nanopipet voltammograms with various contamination degrees at the nanopipet interface from clean (red solid line) to fully contaminated (gray solid line). The TBA^+ IT studied in the negative potential scan was used to characterize and confirm the nanopipet performance, while CO_3^{2-} IT was monitored in the positive potential scan for the study of an FIT. Corresponding pipets were filled with a *premade* 30 mM ionophore solution. (b) Control experiment with a *clean* nanopipet (laminar flow and Ni/Cu inner reference electrode (RE)) filled with a *freshly prepared* 30 mM ionophore solution. Within the fifth running, a nanopipet is blocked. The scan rate is 25 mV/s. All ionophore solutions were vortexed for 15 min.

reproducibly without a notable blockage of nanopipet electrodes in repetitive measurements (ca 80% success rate with $n > 50$, data not shown). These reproducible voltammetric data validate our theoretical speculations on both the slow dissolution rate of the lipophilic bulky ionophore and the peculiar solubility of the ion−ionophore complex at the nanoscale interface.

3.2. Activation of an Ionophore with Hydrated Carbonyl Centers in the Trifluoroacetyl Group. The reduced concentration of the CO_3^{2-} ionophore in the DCE solution clearly mitigates the blockage of the nanopipet interface during nanopipet voltammetry, thus proving an effect of ionophore solubility on the performance of nano-ISEs. However, nanopipets filled with a freshly prepared ionophore solution could not effectively drive FITs regardless of the concentration of the CO_3^{2-} ionophore in the DCE solution, whereas the use of a premade ionophore solution enabled the CO_3^{2-} FITs (Figure S5). This behavior cannot be explained by either solubility or dissolution rate. Indeed, the aging of the DCE solution for 12 h seems to be critical to make CO_3^{2-} FITs possible. Herein, we hypothesized that the aging of the carbonate ionophore solution forms a hydrated ionophore in which a hydrated carbonyl center of the trifluoroacetyl group is an active form to readily bind with CO_3^{2-} during interfacial ion transfer (Figures 3d and S1). Earlier, the hydrated form of carbonate ionophore VII before complexing with CO_3^{2-} has been reported by the Nam group with their fast atom bombardment mass spectroscopic study.[27]

We conducted ^{19}F NMR and ^1H NMR with a freshly prepared ionophore solution and monitored the spectra changes with time to determine if hydration occurs in this mixture. There was inappreciable moisture present in the original NMR sample, so we performed a time study on both the ionic liquid and the ionophore together (i.e., a similar composition to a DCE filling solution) to observe if hydration occurs in this mixture. There was no appreciable change over time (Figure S6a,b). One small but notable feature of the ^1H spectrum of the freshly prepared ionophore solution is the appearance of a secondary, equivalent resonance within the aromatic region with a lower intensity. This resonance appearing at 7.7−8.0 ppm expected from the *gem*-diol product is substantially upfield from the predominant species of ketone seen from 8.1 to 8.4 ppm.[55] There is a similar low-intensity but substantially upfield resonance at 85 ppm present in the ^{19}F spectrum of the freshly prepared ionophore solution. Comparing our spectra to others of compounds synthesized bearing similar *gem*-diol moieties, we see that the low-intensity resonance at 85 ppm on our ^{19}F has a similar chemical shift to the reported one.[56,57] To further confirm if these low-intensity resonances are the *gem*-diol, we spiked the solution with excess water (1−2 water drops added to a 500 μL NMR sample containing 30 mM CO_3^{2-} ionophore in DCE). Though it is not as apparent in the ^1H, the low-intensity resonance at 85 ppm in the ^{19}F dramatically increases in intensity upon addition of water (Figure S6c,d). Comparing this spectrum to that of the freshly prepared ionophore solution, we estimate that the *gem*-diol has converted to about 20% (from the integrated peak area), where the freshly prepared solution had *gem*-diol converted to approximately 6% (Figure S6e,f). The appearance of the *gem*-diol even in the freshly prepared sample occurs due to an equilibrium between the ketone and the hydrated form, where the addition of excess water to the sample pushes the equilibrium toward the formation of more *gem*-diol. Overall, our NMR data and additional voltammetric studies confirmed that the activation of the ionophore with forming hydrated carbonyl centers in the trifluoroacetyl group during aging could be a crucial factor to steadily drive facilitated interfacial ion transfers.

3.3. Cleanness at the Organic/Water Nanoscale Interface. Despite the adequate control of dissolution, solubility, and preactivation of CO_3^{2-} ionophores in the DCE solution, we sometimes struggled with reproducibility in electrochemical measurements of CO_3^{2-} FITs. As an active area of a nanopipet electrode is a nanoscale interface, the cleanness at the interface is critical to accurately probe IT reactions, which can be another key factor to manage the overall reproducibility in measurements. Two major sources of adventitious contamination on the interface are further considered such as an inner reference electrode inserted through the back of a nanopipet and particulate contaminants from the ambient air outside of a nanopipet.

Quartz nanopipets pulled by a CO_2-laser puller have a long taper; thereby, an etched Pt wire is used as an inner reference electrode to be brought to ca 200 μm from the nanopipet interface with tens of nanometer inner radii.[23−25] The shorter the distance between a Pt inner reference electrode and the interface, the smaller the obtained resistance of a nanopipet electrode. A 1 cm long etched Pt is attached to a long Ni/Cu

https://doi.org/10.1021/acs.analchem.2c02626
Anal. Chem. 2023, 95, 4271−4281

(or tungsten) wire glued with Ag epoxy, and this total composite is inserted into a nanopipet and located near the interface to drive an interfacial potential against an outer reference electrode.[16,23] Here, unwanted contamination at the interface can happen from nanoscale fractures or debris of cured Ag epoxy, which can partially or totally block the interface and affect the resulting interfacial ITs. Accordingly, a Pt/Ni−Cu/Ag composited electrode was replaced with a Ni/Cu alloy wire after direct electrochemical etching in concentrated nitric acid/acetic acid etchant (see the Supporting Information). The Ni/Cu alloy is chemically and electrochemically stable, thus being utilized as an electrode.[58−60] The etched Ni/Cu electrode has a similar geometry of a long and lean conical shape with a smooth surface to that of an etched Pt wire, thus being located within 200 μm from a nanopipet interface and retaining a clean liquid/liquid interface free from nanoscale debris.

Further, particulate contaminants from the ambient air could be controlled to keep a nanopipet interface clean by employing the laminar flow, which predictably sweeps particles in a uniform direction from the cleanest area under the hood (i.e., the filter face) to the exit area (i.e., the front opening) (Figure S3). Particularly, we introduced a vertical laminar flow cabinet equipped with a high-efficiency particulate air (HEPA) filter above the standard bench top, where room air enters the system from above the HEPA filter and particle-free air is forced downward toward the work surface. All nanopipet electrodes were handled under the vertical laminar flow, which could be more advantageous than a horizontal one as it reinforces the effect of gravity and efficiently sweeps particles out of the enclosure generally through a front access area.[61]

In Figure 4, voltammograms with both contaminated and clean nanopipets are shown, where discontinuous, capacitive, and almost blocked current responses are observed from contaminated nanopipets (gray and black solid lines). These contaminated nanopipets were prepared in ambient air with an etched Pt wire as an inner reference electrode and a premade CO_3^{2-} ionophore solution. Since the management of contamination degree was out of control, we observed variably blocked currents, which are defined as either partially or totally contaminated status at the nanopipet interface based on the continuity and magnitude of ionic current responses. For example, a totally contaminated nanopipet could drive neither a simple TBA^+ IT nor a CO_3^{2-} FIT across the DCE/water interface due to the complete blockage (black solid curves during forward scans in Figure 4a), whereas a partially contaminated one showed discontinuous current responses for both TBA^+ and CO_3^{2-} Its, indicating a partial blockage (gray solid lines during forward scans in Figure 4). Only nanopipets prepared in the laminar flow cabinet with an etched Ni/Cu electrode and a premade ionophore solution could exclude two sources of adventitious contaminations and acquire retraceable quasi-reversible voltammograms for both CO_3^{2-} FIT and simple TBA^+ IT (red solid curves, background subtracted in Figure 4). The reproducibility of nanopipet electrodes for both CO_3^{2-} and TBA^+ ITs reached nearly 100% (n > 60, data shown in the Supporting Information, Figures S6, S7, and S9). As a control, we tested nanopipets which were fabricated under the clean system with an etched Ni/Cu electrode and filled with a freshly prepared ionophore solution. In this case, we reproducibly observed discontinuous or blocked current responses, i.e., 100% failures in CO_3^{2-} FITs due to the blockage of the nanopipet interface (Figure 4b). Markedly, the inherent cleanness of the nanopipets was controlled as follows: (1) quartz capillaries were blown with compressed air before pulling, (2) the subsequent as-pulled pipets were cleaned with plasma cleaner prior to the silanization process, and (3) silanized pipets were stored under the N_2 gas until their usage.

3.4. Electrochemical Mechanism and Kinetics of a Facilitated CO_3^{2-} Ion Transfer. We quantitatively evaluated experimental voltammograms of a CO_3^{2-} FIT by the finite element analysis to verify the FIT kinetics and mechanism. For the interfacial ion transfer, we can consider two mechanisms, electrochemical ion transfer followed by complexation between the ion and ionophore (i.e., EC mechanism) and concerted electrochemical ion transfer (i.e., E mechanism). We numerically analyzed the experimental voltammograms with theoretical simulations based on EC mechanism as below

$$CO_3^{2-}(w) \underset{k_{i,b}}{\overset{k_{i,f}}{\rightleftarrows}} CO_3^{2-}(org) \tag{3}$$

$$CO_3^{2-}(org) + L(org) \underset{k_d}{\overset{k_a}{\rightleftarrows}} CO_3^{2-}\cdot L\ (org) \tag{4}$$

where L is the CO_3^{2-} ionophore, which interacts selectively with CO_3^{2-} to form a 1:1 complex,[27] and $k_{i,f}$ and $k_{i,b}$ are first-order heterogeneous rate constants for forward and reverse simple interfacial ion transfers, respectively. The rate constants are given by Butler−Volmer relations as[62,63]

$$k_{i,f} = k_i^0 \exp\left[-\frac{\alpha z F(E - E_i^{0'})}{RT}\right] \tag{5}$$

$$k_{i,b} = k_i^0 \exp\left[\frac{(1-\alpha) z F(E - E_i^{0'})}{RT}\right] \tag{6}$$

Also, k_a and k_d are association and dissociation rate constants, respectively. In the presence of an excess amount of ionophore (30 mM), the homogeneous rate constants are related to as below

$$\beta_n = \frac{L_T^n k_a}{k_d} = \frac{k_a'}{k_d} \tag{7}$$

where k_a' is defined as a pseudo-first order rate constant.

Especially, the thermodynamic parameter β_n is directly related with the electrochemical parameter, i.e., potentials as below[16]

$$E^{0'} = E_i^{0'} + \frac{RT}{zF} \ln \beta_n L_T^n \tag{8}$$

where $E_i^{0'}$ is the formal potential of the simple IT.

With a reported formation constant of the TFAB derivatives and the carbonate ion, log β_n = 14.4 ± 0.2,[64] we could obtain the rate constant of ion−ionophore association, k_a = 3.33 × 10^{20} M^{-1} s^{-1}, and the standard rate constant of a simple carbonate ion transfer, k^0 = 35 cm/s (Figure S11 and Table S7, Supporting Information). Notably, the obtained k_a is extremely large compared to the diffusion limited value of $k_{a,d}$ = ∼10^{10} M^{-1} s^{-1} (see the Supporting Information, eq S30).[16] Also, the estimated k^0 = 35 cm/s of the simple carbonate ion transfer is unrealistically high compared to the simple TBA^+ transfer rate, k^0 = 3.6 cm/s, determined by nanopipet voltammetry. These two facts enable us to exclude the possibility of the EC mechanism.

https://doi.org/10.1021/acs.analchem.2c02626
Anal. Chem. 2023, 95, 4271−4281

Accordingly, we mainly consider the E mechanism for the given CO_3^{2-} FIT, where interfacial CO_3^{2-} ion transfer is accompanied with complexation of the ionophore as well as water-finger formation/dissociation as well

$$CO_3^{2-}(w) + L(org) \rightleftarrows CO_3^{2-}\cdot L\,(org) \quad (9)$$

In the presence of an excess amount of ionophores, an FIT can be further treated as a pseudo-first-order process as follows

$$CO_3^{2-}(w) \underset{k_b}{\overset{k_f}{\rightleftarrows}} CO_3^{2-}\cdot L\,(org) \quad (10)$$

where k_f and k_b are first-order heterogeneous rate constants for forward and reverse transfers, respectively. The rate constants are given by Butler–Volmer relations as[63,63]

$$k_f = k^0 \exp\left[-\frac{\alpha z F(E - E^{0'})}{RT}\right] \quad (11)$$

$$k_b = k^0 \exp\left[\frac{(1-\alpha) z F(E - E^{0'})}{RT}\right] \quad (12)$$

where E is the potential applied to a nanopipet electrode against an outer reference electrode, the formal potential, $E^{0'}$, is the potential at $k_f = k_b$, α is the transfer coefficient, z is the charge of a transferred ion, F is the Faraday constant, and k^0 is the standard rate constant.

We could obtain the standard rate constant of CO_3^{2-} FIT, k^0 = 0.048 cm/s, with α and $E^{0'}$. The experimental voltammogram (black solid curves, background subtracted) fits well with the simulated quasi-reversible voltammogram (red open circles), yielding k^0 = 0.048 cm/s, α = 0.45, z = −2, $E^{0'}$ = 0.365 V vs Pt QRE (or 0.232 V vs $E_{1/2,TBA}$), and γ (i.e., $D_{complex,DCE}/D_{CO_3^{2-},aq}$) = 0.68 (Figure 5). Notably, α = 0.45 is close to a normal value of 0.5, indicating the one-step mechanism of the electrochemical interfacial IT reaction.[62]

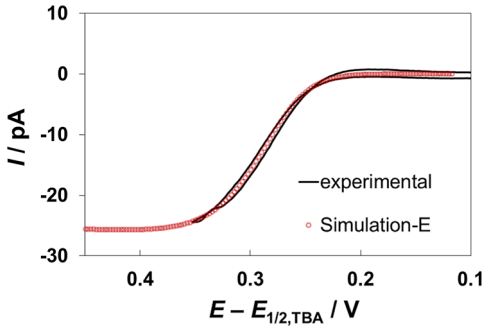

Figure 5. Steady-state voltammogram of CO_3^{2-} FITs across the DCE/water interface obtained with a nanopipet filled with a *premade* 30 mM ionophore solution. Ionophore solutions were vortexed for 15 min. The best theoretical fitting (red open circles) to the experimental curves (black solid curves, background subtracted forward wave) was calculated from simulations with COMSOL Multiphysics using parameters in the Supporting Information. The scan rate is 25 mV/s.

More interestingly, our obtained k^0 value with a given β = 10^{14} is similar to the rate constants obtained with non-covalent-bond forming ionophores (e.g., for Ag^+, k^0 = 0.026 cm/s, $\beta = 2.5 \times 10^{12}$, and for K^+, k^0 = 0.011 cm/s, $\beta = 6.3 \times 10^{14}$) measured by micropipet voltammetry.[16] Previously, Nam, Meyerhoff, and Simon reported the covalent bond formation between CO_3^{2-} and the ionophore of trifluoroacetophenone derivatives.[27,65] If this covalent bond formation is strong, the ion–ionophore association/dissociation rate would become significantly slow;[66] thereby, the interfacial ion transfer would not be observable in fast nanopipet voltammetry. In fact, our nanopipet voltammetry work is the first successful case with covalent bond-forming ionophores for FITs. Herein, the similarity of k^0 and β values between the non-covalent bond-forming ionophore and CO_3^{2-} ionophore VII with forming covalent bonds implies that weak binding of the CO_3^{2-}-ionophore and CO_3^{2-} results in fairly fast association/dissociation of the ion–ionophore complex, thereby enabling the facilitated ion transfer within the reasonable potential window in fast nanopipet voltammetry. In that sense, instead of the nature of bonding between the ion and ionophore, the strength of the bonding could determine the feasibility and applicability of the ionophore in the FIT study by nanopipet voltammetry.

3.5. Quantification of CO_3^{2-} Produced by *S. oneidensis* MR-1. We further demonstrate the analytical utility of amperometric nano-CO_3^{2-} ISEs by in situ measuring the actual level of CO_3^{2-} produced by MRB as a result of organic fuel oxidation. Dissimilar MRB such as *S. oneidensis* MR-1 use organic waste molecules, e.g., acetate or lactate as food, oxidize them, and produce CO_3^{2-} and electrons as metabolic wastes.[30] Accordingly, sensing and quantification of total CO_3^{2-} amount enable us to monitor the performance of MRB with respect to organic fuel oxidation, i.e., production of electrons as a promising anode material in MFCs.[40,40]

$$\text{carbon sources} \rightarrow CO_2(aq) + H_2O \rightleftarrows HCO_3^-(aq) + H^+ \rightleftarrows CO_3^{2-}(aq) + 2H^+ \quad (13)$$

In the practical application of nano-CO_3^{2-} ISEs to biological systems, a critical factor is biofouling. We conducted voltammetry and amperometry in bacterial growth media and modified M-1 medium prepared with piperazine-*N*,*N*′-bis(2-ethanesulfonic acid) (PIPES) buffer containing 30 mM acetate or lactate as a carbon source and other growth nutrients. None of the noticeable signs of biofouling was seen for either TBA^+ or CO_3^{2-} IT reactions in the supernatant of growth media used for bacterial incubation. Neither decrease in the current nor blockage of nanopipet responses was observed during measurements (Figure S7).

In order to quantify the intrinsic CO_3^{2-} present in the supernatant of bacterial growth media, the concentration of CO_3^{2-} is directly estimated from the current in the obtained voltammogram. Without background subtraction, a direct current at $E - E_{1/2,TBA}$ = 0.3 V in a pristine voltammogram shows a negligible contribution of the background, which corresponds to ∼73% of an anticipated limiting current (at $E - E_{1/2,TBA}$ = 0.35 V) in a background-subtracted voltammogram (Figures 5 and 6a). Therefore, we selected a direct current, 5.0 ± 0.3 pA at $E - E_{1/2,TBA}$ = 0.3 V, and multiplied a 1.36 factor to compensate for a deviation from 100% of a limiting current. Subsequently, using a limiting current equation, we could directly estimate a concentration of CO_3^{2-} produced by bacteria. A limiting current (i_{lim}) is linearly proportional to the concentration of CO_3^{2-} as below[67]

$$i_{lim} = 4xzFDCr \quad (14)$$

where x is an RG factor (a ratio of the outer/inner radii of the nanopipet, x = 1.15 for RG 1.6), z is a unit charge of the

https://doi.org/10.1021/acs.analchem.2c02626
Anal. Chem. 2023, 95, 4271−4281

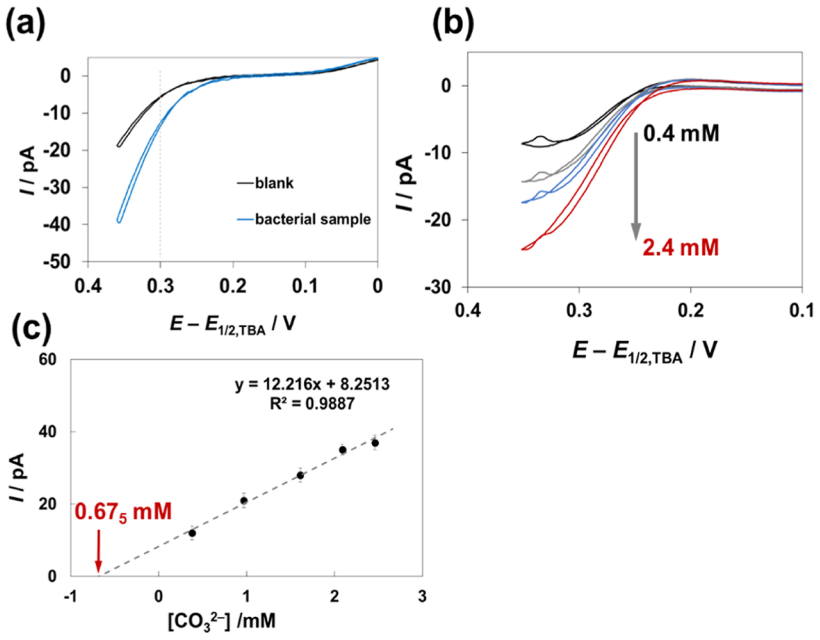

Figure 6. (a) Original voltammograms in blank (black solid curves) and bacterial growth media (blue solid curves). (b) Background-subtracted voltammograms with a CO_3^{2-}-selective nanopipet ITIES electrode filled with a *premade* 30 mM carbonate ionophore VII solution, which were measured in a modified M-1 medium containing 0.4−2.4 mM standard CO_3^{2-} spikes. The scan rate is 25 mV/s. The ionophore solutions were vortexed for 15 min. (c) Calibration plot constructed with the standard addition method for CO_3^{2-} quantification measured by CO_3^{2-} ion-selective nanopipet voltammetry with *S. oneidensis*-grown buffer media containing acetate or lactate as a carbon source. An *x*-intercept gives the value of the original concentration of CO_3^{2-} as $0.67_5 \pm 0.03$ mM ($n = 5$) produced by *S. oneidensis*.

analyte ion ($z = -2$), F is the Faraday constant (96485 C/mol), D and C are the diffusion coefficient and concentration of the analyte ion, respectively, and r is the inner radius of a nanopipet opening. The direct quantification of the CO_3^{2-} concentration gives 0.70 ± 0.04 mM from the pristine voltammogram without background subtraction.

Further, this CO_3^{2-} concentration is validated by the standard addition method,[45] where a known amount of CO_3^{2-} spikes was sequentially added, and voltammetry was subsequently performed (Figure 6b). Particularly, the standard addition method is useful to consider a matrix effect in our measurement in the presence of various anion interferents in growth media, e.g., $H_2PO_4^-$, Cl^-, and SO_4^{2-} (more details are in the Supporting Information). Herein, limiting currents from background-subtracted voltammograms were used to construct a calibration curve of standard additions (Figure 6b).

As shown in Figure 6c, a linear curve of i_{lim} vs the concentration of CO_3^{2-}, $C_{CO_3^{2-}}$ is obtained, where a slope contains information of $D_{CO_3^{2-}\,aq}$, and the *x*-intercept gives the original concentration of CO_3^{2-} in growth media produced by *S. oneidensis*.[45] In the presence of each carbon source of acetate and lactate, the resulting concentrations of CO_3^{2-} are $0.67_5 \pm 0.03$ and 0.70 ± 0.04 mM (data not shown), respectively. Also, in modified M-1 media containing lactate as a carbon source and fumarate for the anaerobic condition, the determined CO_3^{2-} was 0.75 ± 0.03 mM (Figure S5b). Diffusion coefficients of CO_3^{2-} in M-1 media containing acetate or lactate are 1.83×10^{-6} and 1.70×10^{-6} cm^2/s, respectively. Earlier, DiChristina and co-workers reported a maximum of 0.20 mM of total dissolved inorganic carbon (sum of aqueous species of CO_2, HCO_3^-, and CO_3^{2-}) produced from ^{13}C-acetate during acetate oxidation by the *Shewanella* strain, MN01, measured by liquid chromatography-isotope ratio mass spectrometry.[68] Our in situ estimation of the CO_3^{2-} concentration shows a similar order of magnitude, while a small difference would be due to different amounts of bacteria.

Notably, our amperometric nano-CO_3^{2-} ISEs will open up the applicability to the nanoelectrochemical approach such as nanoscale SECM to directly probe CO_3^{2-} as a result of an organic fuel oxidation by a single living bacterium. Also, this nanopipet electrode will be broadly useful for the study of electrocatalytic and photocatalytic reactions that produce or consume carbon dioxide in water.

4. CONCLUSIONS

In this work, we showed the successful demonstration and application of CO_3^{2-}-selective amperometric/voltammetric probes using nanopipet-supported ITIES and broadly available Simon-type ionophores. Especially, this is the first successful study of nanopipet voltammetry using an ionophore forming covalent bonding with an ion. We revealed critical factors governing the overall performance of CO_3^{2-} nano-ISEs such as slow dissolution of bulky ionophores in the organic phase, activation of hydrated ionophores, distinct solubility of the ion−ionophore complex in the organic phase near the interface, and the cleanness at the nanoscale interface. The adequate experimental control of these factors leads to reproducible voltammogram data and reliable theoretical assessment, confirming the one-step E mechanism, where an interfacial ion transfer is concerted with a complexation of ion−ionophore. Notably, the obtained rate constant, k^0 = 0.048 cm/s, is very similar to rates of other FIT reactions using ionophores forming non-covalent bonds with ions. This result clearly implies that a weak binding between the CO_3^{2-} ion and ionophore enables to observe FITs by fast nanopipet voltammetry regardless of the nature of bonding between the ion and ionophore. The analytical utility of amperometric

https://doi.org/10.1021/acs.analchem.2c02626
Anal. Chem. 2023, 95, 4271−4281

nano-CO_3^{2-} ISEs is further demonstrated by in situ measuring CO_3^{2-} produced by *S. oneidensis* MR-1 via organic fuel oxidation. We will further employ a newly demonstrated amperometric nano-CO_3^{2-} ISE with SECM to study organic fuel oxidation at a single bacterial cell with high spatial and temporal resolution. Importantly, our finding can be broadly applied to develop various types of amperometric/voltammetric nanoprobes utilizing ion−ionophore recognition for clinical, physiological, industrial, and environmental analysis as well.

■ ASSOCIATED CONTENT

Supporting Information

The Supporting Information is available free of charge at https://pubs.acs.org/doi/10.1021/acs.analchem.2c02626.

Modified M-1 medium; *Shewanella* federation recipe; structure of carbonate ionophore VII and its complex with CO_3^{2-}; experimental section; picture of a vertical laminar flow clean cabinet; cyclic voltammograms with and without CO_3^{2-} ionophore VII; nanopipet voltammetry with nanopipets filled with 5 mM CO_3^{2-} ionophore VII solutions; NMR study to confirm the hydration of trifluoroacetyl carbon centers in CO_3^{2-} ionophore VII for activation; amperometric *i*−*t* curves for the fouling test of nanopipet electrodes in the M-1 medium used for bacterial incubation; calibration curve for the standard addition method; MOE simulation report (MD simulation); selectivity tests; and reversibility tests (PDF)

Detailed COSMOL model report on the E mechanism and EC mechanism and fine element simulation by COMSOL multiphysics (I. E mechanism and II. EC mechanism) (PDF)

■ AUTHOR INFORMATION

Corresponding Author

Jiyeon Kim − *Department of Chemistry, University of Rhode Island, Kingston, Rhode Island 02881, United States;* orcid.org/0000-0002-7624-6766; Phone: +1 (401) 874-2143; Email: jkim25@uri.edu

Authors

Subhashini Elangovan − *Department of Chemistry, University of Rhode Island, Kingston, Rhode Island 02881, United States*

Surendra Raj Puri − *Department of Chemistry, University of Rhode Island, Kingston, Rhode Island 02881, United States*

Hiranya Madawala − *Department of Chemistry, University of Rhode Island, Kingston, Rhode Island 02881, United States*

Justin Pantano − *Department of Chemistry, University of Rhode Island, Kingston, Rhode Island 02881, United States;* orcid.org/0000-0001-8115-8974

Brett Pellock − *Department of Biology, Providence College, Providence, Rhode Island 02981, United States*

Matthew K. Kiesewetter − *Department of Chemistry, University of Rhode Island, Kingston, Rhode Island 02881, United States;* orcid.org/0000-0001-5475-1246

Complete contact information is available at: https://pubs.acs.org/10.1021/acs.analchem.2c02626

Author Contributions

S.E. and S.P. contributed to this work equally. J.K. designed the experiments and interpreted all the data. S.P. and S.E. conducted electrochemical experiments and analyzed the data. H.M. performed MD simulation. J.P. and M.K. performed NMR measurements and interpreted the NMR results. B.P. provided bacterial samples and discussed the electrochemical results with J.K. S.E. has contributed to the initial draft preparation but has been unreachable and did not participate in the peer review of this manuscript. All authors except S.E. have given approval to the final version of the manuscript.

Notes

The authors declare no competing financial interest.

■ ACKNOWLEDGMENTS

This work was supported by the National Science Foundation (CHE-2046363), the Research Bridge Funding Initiative, start-up fund from University of Rhode Island, Medical Research Fund (20174373) from Rhode Island Foundation, and in part by the Rhode Island Institutional Development Award (IDeA) Network of Biomedical Research Excellence from the National Institute of General Medical Sciences of the National Institutes of Health (P20GM103430). The provision of the Bruker ASCEND 400 MHz spectrometer at the Teknor-Apex laboratory is supported by the Chemistry department at the University of Rhode Island.

■ REFERENCES

(1) Meyerhoff, M. E. Electrochemistry and chemical sensors. In *Tietz Textbook of Clinical Chemistry and Molecular Diagnostics*; Burtis, C. A., Ashwood, E. R., Bruns, D. E., Eds.; Elsevier Saunders: St. Louis, MO, 2011, p 259.

(2) Fry, C. H.; Langley, S. E. M. *Ion-selective Electrodes for Biological Systems*; Harwood Academic Publishers: Amsterdam, Netherlands, 2001.

(3) Arrigan, A. W. M.; Arrigan, E. A. E.; Liu, Y. *Aust. J. Chem.* **2016**, *69*, 1016−1032.

(4) Zuliani, C.; Diamond, D. *Electrochim. Acta* **2012**, *84*, 29.

(5) Bakker, E.; Bühlmann, P.; Pretsch, E. *Chem. Rev.* **1997**, *97*, 3083−3132.

(6) Amemiya, S. Potentiometric Ion-Selective Electrodes. In *Handbook of Electrochemistry*; Zoski, C. G., Ed.; Elsevier: New York, 2007, pp 261−294. DOI: 10.1016/b978-044451958-0.50020-3

(7) Young, C. C. *J. Chem. Educ.* **1997**, *74*, 177−182.

(8) Fry, C. H.; Langley, S. E. M. *Ion-Selective Electrodes for Biological Systems*; Harwood Academic Publishers: Amsterdam, The Netherlands, 2001.

(9) Senda, M.; Kakiuchi, T.; Osaka, T. *Electrochim. Acta* **1991**, *36*, 253−262.

(10) Samec, Z.; Samcová, E.; Girault, H. H. *Talanta* **2004**, *63*, 21−32.

(11) Henn, D.; Cammann, K. *Electroanalysis* **2000**, *12*, 1263−1271.

(12) Muslinkina, L.; Pretsch, E. *Chem. Commun.* **2004**, 1218−1219.

(13) Muslinkina, L.; Pretsch, E. *Electroanalysis* **2004**, *16*, 1569−1575.

(14) Langmaier, J.; Samcová, E.; Samec, Z. *Anal. Chem.* **2007**, *79*, 2892−2900.

(15) Taylor, G.; Girault, H. H. *J. Electroanal. Chem.* **1986**, *208*, 179−183.

(16) Ishimatsu, R.; Izadyar, A.; Kabagambe, B.; Kim, Y.; Kim, J.; Amemiya, S. *J. Am. Chem. Soc.* **2011**, *133*, 16300−16308.

(17) Rodgers, P. J.; Amemiya, S. *Anal. Chem.* **2007**, *79*, 9276−9285.

(18) *Scanning Electrochemical Microscopy*; Bard, A. J., Mirkin, M. V., Eds.; Marcel Dekker: New York, 2001.

(19) Shao, Y.; Mirkin, M. V. *J. Am. Chem. Soc.* **1997**, *119*, 8103−8104.

(20) Yuan, Y.; Shao, Y. H. *J. Phys. Chem. B* **2002**, *106*, 7809−7814.
(21) Cai, C. X.; Tong, Y. H.; Mirkin, M. V. *J. Phys. Chem. B* **2004**, *108*, 17872−17878.
(22) Jing, P.; Zhang, M. Q.; Hu, H.; Xu, X. D.; Liang, Z. W.; Li, B.; Shen, L.; Xie, S. B.; Pereira, C. M.; Shao, Y. H. *Angew. Chem., Int. Ed.* **2006**, *45*, 6861−6864.
(23) Shen, M.; Ishimatsu, R.; Kim, J.; Amemiya, S. *J. Am. Chem. Soc.* **2012**, *134*, 9856−9859.
(24) Chen, R.; Balla, R. J.; Lima, A.; Amemiya, S. *Anal. Chem.* **2017**, *89*, 9946−9952.
(25) Chen, R.; Yang, A.; Chang, A.; Oweimrin, P. F.; Romero, J.; Vichitcharoenpaisarn, P.; Tapia, S.; Ha, K.; Villaflor, C.; Shen, M. *ChemElectroChem* **2020**, *7*, 967−974.
(26) Bakker, E. *Chimia* **2020**, *74*, 569−576.
(27) Lee, H. J.; Yoon, I. J.; Yoo, C. L.; Pyun, H.-J.; Cha, G. S.; Nam, H. *Anal. Chem.* **2000**, *72*, 4694−4699.
(28) Xie, X.; Pawlak, M.; Tercier-Waeber, M.-L.; Bakker, E. *Anal. Chem.* **2012**, *84*, 3163−3169.
(29) Shao, Y.; Osborne, M. D.; Girault, H. H. *J. Electroanal. Chem.* **1991**, *318*, 101−109.
(30) Wang, D.; Pan, J.; Xu, M.; Liu, B.; Hu, J.; Hu, S.; Hou, H.; Elmaadawy, K.; Yang, J.; Xiao, K.; Liang, S. *J. Power Source* **2021**, *483*, 229220.
(31) Welch, A. J.; Dunn, E.; DuChene, J. S.; Atwater, H. A. *ACS Energy Lett.* **2020**, *5*, 940−945.
(32) Athavale, R.; Pankratova, N.; Dinkel, C.; Bakker, E.; Wehrli, B.; Brand, A. *Environ. Sci. Technol.* **2018**, *52*, 11259−11266.
(33) Jansod, S.; Ghahraman Afshar, M. G.; Crespo, G. A.; Bakker, E. *Anal. Chem.* **2016**, *88*, 3444−3448.
(34) Cuartero, M.; Pankratova, N.; Cherubini, T.; Crespo, G.; Massa, F.; Confalonieri, F.; Bakker, E. *Environ. Sci. Technol.* **2017**, *4*, 410−415.
(35) Jarolímová, Z.; Bosson, J.; Labrador, G. M.; Lacour, J.; Bakker, E. *Electroanalysis* **2018**, *30*, 1378−1385.
(36) Jarolímová, Z.; Crespo, G. A.; Xie, X.; Ghahraman Afshar, M. G.; Pawlak, M.; Bakker, E. *Anal. Chem.* **2014**, *86*, 6307−6314.
(37) Jansod, S.; Ghahraman Afshar, M. G.; Crespo, G. A.; Bakker, E. *Anal. Chem.* **2016**, *88*, 3444−3448.
(38) Choi, Y. S.; Lvova, L.; Shin, J. H.; Oh, S. H.; Lee, C. S.; Kim, B. H.; Cha, G. S.; Nam, H. *Anal. Chem.* **2002**, *74*, 2435−2440.
(39) Santoro, C.; Arbizzani, C.; Erable, B.; Ieropoulos, I. *J. Power Source* **2017**, *356*, 225−244. (b) Lovely, D. R. *Annu. Rev. Microbiol.* **2012**, *66*, 391−409.
(40) Lovely, D. R. *Annu. Rev. Microbiol.* **2012**, *66*, 391−409.
(41) Kikkawa, N.; Wang, L.; Morita, A. *J. Am. Chem. Soc.* **2015**, *137*, 8022−8025.
(42) Koizumi, A.; Tahara, H.; Hirano, T.; Morita, A. *J. Phys. Chem. Lett.* **2020**, *11*, 1584−1588.
(43) Amemiya, S. *Anal. Chem.* **2016**, *88*, 8893−8901.
(44) Guo, J.; Amemiya, S. *Anal. Chem.* **2006**, *78*, 6893−6902.
(45) Harris, D. C. *Quantitative Chemical Analysis*, 9th ed., W. H. Freeman and Company, 2016; pp 106−109.
(46) Gao, Y.; Glennon, B.; He, Y.; Donnellan, P. *ACS Omega* **2021**, *6*, 8056−8067.
(47) Evoy, E.; Maclean, A. M.; Rovelli, G.; Li, Y.; Tsimpidi, A. P.; Karydis, V. A.; Kamal, S.; Lelieveld, J.; Shiraiwa, M.; Reid, J. P.; Bertram, A. K. *Atmos. Chem. Phys.* **2019**, *19*, 10073−10085.
(48) Amemiya, S.; Wang, Y.; Mirkin, M. V. Nanoelectrochemistry at the liquid/liquid interfaces. In *Specialist Periodical Reports in Electrochemistry*, Compton, R., Wadhawan, J., Eds.; RSC Publishing, 2013; Vol. *12*, pp 1−43.
(49) Fileti, E.; Chaban, V. *Phys. Chem. Chem. Phys.* **2017**, *19*, 3903−3910.
(50) Ghadar, Y.; Parmar, P.; Samuels, A. G.; Clark, A. E. *J. Chem. Phys.* **2015**, *142*, 104707.
(51) Holmberg, N.; Sammalkorpi, M.; Laasonen, K. *J. Phys. Chem. B* **2014**, *118*, 5957−5970.
(52) Liang, Z.; Bu, W.; Schweighofer, K. J.; Walwark, D. J., Jr.; Harvey, J. S.; Hanlon, G. R.; Amoanu, D.; Erol, C.; Benjamin, I.; Schlossman, M. *Proc. Natl. Acad. Sci. U.S.A.* **2019**, *116*, 18227−18232.
(53) Qiao, B.; Muntean, J. V.; Olvera de la Cruz, M.; Ellis, R. J. *Langmuir* **2017**, *33*, 6135−6142.
(54) Puri, S. R.; Kim, J. *Anal. Chem.* **2019**, *91*, 1873−1879.
(55) Carey, F. A.; Giuliano, R. M. *Organic Chemistry*, 10th ed.; McGraw Hill Publishing Company, 2017.
(56) Linderman, R. J.; Graves, D. M. *J. Org. Chem.* **1989**, *54*, 661−668.
(57) Hazlitt, R. A.; John, J. P.; Tran, Q.; Colby, D. A. *Tetrahedron Lett.* **2016**, *57*, 1906−1908.
(58) ASM. *Metals Handbook*, 9th ed.; ASM: Metals Park, Ohio, 1981.
(59) Yeo, I.-H.; Johnson, D. C. *J. Electroanal. Chem.* **2001**, *495*, 110−119.
(60) Li, A.; Binnemans, K. *Chem. Rev.* **2021**, *121*, 4506−4530.
(61) Horizontal or Vertical Laminar Flow Clean Bench | Air Science.
(62) Samec, Z.; Homolka, D.; Mareček, V. *J. Electroanal. Chem.* **1982**, *135*, 265.
(63) Samec, Z. *Pure Appl. Chem.* **2004**, *76*, 2147.
(64) Makarychev-Mikhailov, S.; Legin, A.; Mortensen, J.; Levitchev, S.; Vlasov, Y. *Analyst* **2004**, *129*, 213−218.
(65) Meyerhoff, M. E.; Pretsch, E.; Welti, D. H.; Simon, W. *Anal. Chem.* **1987**, *59*, 144−150.
(66) Savéant, J.-M. *J. Am. Chem. Soc.* **1987**, *109*, 6788−6795.
(67) Bard, A. J.; Faulkner, L. R., *Electrochemical Methods: Fundamentals and Applications*, 2nd ed., John Wiley & Sons, INC.: NY, 2001, p 174.
(68) Szeinbaum, N.; Lin, H.; Brandes, J. A.; Taillefert, M.; Glass, J. B.; DiChristina, T. J. *Environ. Microbiol.* **2017**, *19*, 3475−3486.

https://doi.org/10.1021/acs.analchem.2c02626
Anal. Chem. 2023, 95, 4271−4281